Particle Yields at the Stanford Linear Accelerator Center and the Photon-Nucleus Interaction in the 5–18-GeV Region*

STANLEY M. FLATTÉ AND JOSEPH J. MURRAY†
Lawrence Radiation Laboratory, University of California, Berkeley, California

AND

PAUL R. KLEIN
Department of Physics, Purdue University, West Lafayette, Indiana

AND

LAWRENCE H. JOHNSTON
Stanford Linear Accelerator Center, Stanford University, Stanford, California

AND

STANLEY G. WOJCICKI
Department of Physics, Stanford University, Stanford, California

(Received 7 August 1967)

Yields of $\pi^{\pm}$, $K^{\pm}$, $p^{\pm}$, and $e^{\pm}$ at 2 and 3 deg from 16- and 18-GeV electrons on three different targets have been measured at the Stanford 2-mile electron accelerator. The targets were: 0.3 radiation length (r.l.) of Be, 0.3 r.l. of Fe, and a combination consisting of 0.6 r.l. of Fe followed by 0.3 r.l. of Be. The yields are discussed in terms of the Drell mechanism (for $\pi^{\pm}$, $K^{\pm}$, $p^{\pm}$), ρ production ($\pi^{\pm}$), associated production from pions produced by photons (K^{+}), photodisintegration (p^{+}), and elastic scattering (e^{-}). The A dependences of the yields have been determined from the ratio of the Be- and the Fe-target yields.

I. INTRODUCTION

THE new 20-GeV Stanford electron accelerator provides a unique opportunity for the study of the photon-nucleus interaction at energies much greater than previously available. Expectations that this new energy region would be interesting were greatly enhanced by Drell,[1] who, in 1960, calculated the amplitudes for a particular set of photon-induced peripheral processes which produce strongly interacting particles. At energies up to 6 GeV it has been found that these peripheral processes account for a large part, though not all, of pion production, and it was anticipated that at higher energies these processes would more completely dominate the cross section for forward angles.[2] As an added fillip, Drell's calculations were used to predict yields of secondary particles at the Stanford Linear Accelerator Center (SLAC) that were large enough to be experimentally useful.[3] Later it was realized that another important mechanism, ρ production, contributes to the $\pi^{\pm}$ yields.[4]

While engaged in an experiment[5] to determine the usefulness of some secondary-particle beams at SLAC, we have gathered data on secondary-particle yields from targets exposed directly to the electron beam. This article differs in substance from Ref. 5 principally in the inclusion of data from an Fe target and an Fe-Be combination target (see Table I). Although the data are by no means complete, we believe that they constitute enough information to allow some useful, though preliminary, conclusions. Basically, the experimental results indicate that, with two notable exceptions, the yields of strongly interacting particles roughly agree with the predictions of the Drell mechanism plus ρ production ("Drell+ρ").

The first exception is the K^{+} yields, which are 1.6–3.7 times the K^{-} yields, where 1.3 is expected from the Drell mechanism. The most logical explanation for the excess K^{+} is the process $\pi p \rightarrow K^{+}\Lambda(\Sigma)$, taking place in the same nucleus where a photon has produced the π; however, no direct evidence of this process is given.[6] The second exception is the proton yields, which are 10 times the $\bar{p}$ yields. Here processes of photodisintegration (where a proton is "knocked out" of the nucleus) are invoked, again with no direct confirmation.[7]

Although the absolute magnitude of the yields does agree reasonably well with Drell+ρ, their momentum and angle dependences are not in quantitative agreement. The effects of final-state interactions will definitely modify the Drell+ρ predictions toward agree-

* Work performed under the auspices of the U. S. Atomic Energy Commission.

† Present address: Stanford Linear Accelerator Center, Stanford University, Stanford, Calif.

[1] S. D. Drell, Phys. Rev. Letters **5**, 278 (1960).

[2] W. A. Blanpied, J. S. Greenberg, V. W. Hughes, D. C. Lee, and R. C. Minehart, Phys. Rev. Letters **11**, 477 (1963); R. B. Blumenthal, W. L. Faissler, P. M. Joseph, L. J. Lanzerotti, F. M. Pipkin, D. G. Stairs, J. Ballam, H. De Staebler, Jr., and A. Odian, *ibid.* **11**, 496 (1963).

[3] J. S. Ballam, W. W. Hansen Laboratories of Physics, Stanford University, M Report No. 200, 1960 (unpublished); S. D. Drell, Rev. Mod. Phys. **33**, 458 (1961); for a more recent review see S. D. Drell, in *Proceedings of the International Symposium on Electron and Photon Interactions at High Energies, Hamburg, 1965*, edited by G. Höhler *et al.* (Deutsche Physikalische Gesellschaft, Hamburg, 1965).

[4] S. M. Berman and S. D. Drell, Phys. Rev. **133**, B791 (1964).

[5] S. M. Flatté, R. A. Gearhart, T. Hauser, J. J. Murray, R. Morgado, M. Peters, P. R. Klein, L. H. Johnston, and S. G. Wojcicki, Phys. Rev. Letters **18**, 366 (1967).

[6] Y. S. Tsai, Stanford Linear Accelerator Center Users Handbook (unpublished).

[7] S. D. Drell (private communication).

TABLE I. Particle yields in particles sr^{-1} $(GeV/c)^{-1}$ per 10^7 incident electrons. Both the Be and Fe targets were 0.3 r.l., but the Be-Fe target consisted of 0.6 r.l. of Fe followed by 0.3 r.l. of Be. The errors reported here are the algebraic sums of the statistical errors and nonstatistical fluctuations described in the text. The over-all normalization of the data is believed to be accurate to ±15%. All yields are at the target, i.e., they have been corrected for decay in flight. The muon fraction, measured at a few momenta, was found to be <1% of the total yield.

Target, primary electron energy, and production angle	Charge and secondary momentum (GeV/c)	Yield: Electron	Yield: Pion	Yield: Kaon	Yield: Proton
Be, 16 GeV,[a] 3 deg	+10		148 ± 6	26 ± 3	10.7 ± 1.7
	+12		35.2± 1.6	10.7± 1.2	3.2 ± 0.3
	−10	252± 12	156 ± 11	10.7± 1.2	1.1 ± 0.2
	−12	299± 9	37 ± 4	2.8± 0.4	0.17± 0.10
Be, 18 GeV,[b] 3 deg	+6		1480 ± 60	103 ±15	126 ±30
	+10		186 ± 8	35 ± 3	15.1 ± 1.8
	+12		64 ± 3	14.2± 1.7	8.0 ± 0.9
	−12	164± 5	52 ± 3	4.3± 0.5	0.26± 0.07
Be, 18 GeV,[b] 2 deg	+4	440± 40	2330 ±100	230 ±30	260 ±80
	+6	98± 12	2130 ± 60	166 ±21	84 ±10
	+8		1630 ± 40	86 ±11	49 ± 4
	+10		900 ± 20	56 ± 3	23.2 ± 1.7
	+12[c]		304 ± 7	31 ± 3	9.8 ± 0.8
	+14		76 ± 2	14.6± 1.5	3.5 ± 0.6
	−4	2780±120	2520 ±150	114 ±10	
	−6	1280± 80	2050 ±100	103 ±11	7.1 ± 1.3
	−8	970± 60	1680 ± 80	49 ± 5	5.1 ± 1.0
	−10	970± 50	820 ± 50	22.5± 2.5	2.9 ± 0.7
	−12	930± 40	280 ± 30	8.3± 0.9	1.2 ± 0.4
	−14	1060± 40	74 ± 26	4.5± 0.7	
Fe, 18 GeV,[b] 2 deg	+4	226± 18	503 ± 27	65 ± 8	82 ±22
	+6	28± 3	512 ± 13	40 ± 5	20 ± 2
	+8		517 ± 12	24 ± 3	11 ± 1
	+10		306 ± 6	14 ± 1	5.4 ± 0.5
	+12		57 ± 1.4	6.2± 0.7	1.6 ± 0.25
	+14		12.2± 0.5	3.7± 0.5	0.55± 0.15
	−4	1410± 65	650 ± 70	49 ± 5	
	−6	400± 24	510 ± 30	25 ± 2.5	
	−8	320± 20	560 ± 30	15 ± 2	1.7 ± 0.3
	−10	275± 15	285 ± 20	4.3± 0.7	0.7 ± 0.2
	−12	286± 12	52 ± 8	2.1± 0.4	0.1 ± 0.1
	−14	316± 6			
Be-Fe, 18 GeV,[b] 2 deg	+6	580±120	5410 ±240	380 ±50	170 ±20
	+8		4930 ±120	250 ±30	146 ±16
	+12		663 ± 17	71 ± 7	24 ± 2.5
	−6	4290±260	5610 ±330	230 ±30	16 ± 2
	−12	1180± 60	580 ± 50	20 ± 3	1.9 ± 0.7

[a] 16.00±0.08 GeV.
[b] 17.85±0.15 GeV.
[c] Deuterons here were found to be less than 3% of the protons.

ment; however, no method of quantitative calculation is known.

In Sec. V we discuss these theoretical questions in more detail, as well as cover the implications of the bremsstrahlung photon spectrum within the target, the A dependences of the yields, and the electron yields.

II. EXPERIMENTAL APPARATUS AND PROCEDURE

A. Primary and Secondary Beams

A beam of electron pulses was provided by the Stanford 20-GeV linear accelerator. The normal pulse rate during the experiment was 180 pulses per sec, with each pulse containing about 10^{10} electrons and lasting 1.5 μsec. The energy of the electrons was 18 GeV (a few runs were at 16 GeV), with an energy spread of <1%. The beam spot size at our target was about 0.3 cm vertically and 0.5 cm horizontally, the larger horizontal dimension arising from some momentum dispersion due to the guiding magnets ahead of our target.

We used three different targets in the experiment. Our basic target was a 10-cm length of beryllium [≈0.3 radiation length (r.l.)]. In order to determine the dependence of the yields on the atomic weight of the target nuclei, we used an iron target with a length of 0.54 cm (≈0.3 r.l., and made to correspond as closely as possible to the number of radiation lengths in 10 cm of Be). The purpose of our third target was more utilitarian: to determine the maximum yield obtainable from a 10-cm-long target. This third target was 10 cm

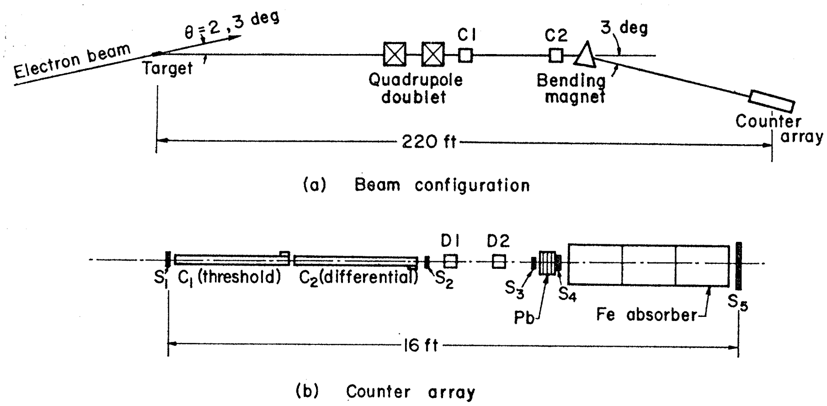

FIG. 1. (a) Beam configuration (not to scale). C1 and C2 are lead collimators. (b) Counter array (not to scale). S_1, S_2, S_3, S_4, and S_5 are plastic scintillators; C_1 and C_2 are, respectively, threshold and differential Čerenkov detectors; D1 and D2 are DCFEM's mentioned in the text.

of Be preceded by 0.95 cm (≈0.6 r.l.) of iron. The interpretation of the results from this target is given in Sec. V B.

The primary-beam monitor system is described in another publication.[8] Briefly, a signal from the target (which was electrically insulated) provided a measure of the net charge leaving the target over any period of time. By comparing the absolute magnitude of the electron beam current, as measured by calibrated toroids, with the electrical signal from the target when all the beam was hitting the target, we obtained an absolute calibration of the target signal. The results were that the Be, Fe, and Be-Fe-combination targets were 125, 21, and 292% efficient, respectively. An efficiency of 100% means that for each electron in the primary beam entering the target, two electrons leave the target (where one of these may, of course, be the primary electron). Since the calibrated toroids on which this measurement was based are accurate to ±5%, the uncertainty in the absolute normalization of the primary electron beam current is ±5%.

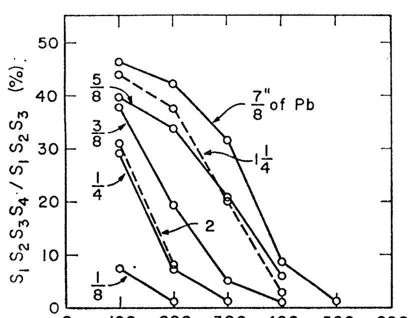

FIG. 2. Development of an electron shower as seen by the shower counter S_4. The S_4 voltage was set so that singles did not register at a 100-mV discriminator setting. The secondary beam momentum was 6 GeV/c, where the Čerenkov counters indicated that 44±2% of the beam were electrons. The "plateau" with $\frac{7}{8}$-in. Pb was poor because of the small multiplicity of the shower at this low energy.

[8] R. A. Gearhart, T. Hauser, L. H. Johnston, P. R. Klein, and J. J. Murray (unpublished).

Figure 1(a) shows the beam layout. The quadrupole doublet focused particles of the desired momentum onto the counter array. The bending magnet provided momentum resolution at the counters. The 3-ft-long lead collimators C1 and C2 defined the solid-angle acceptance in an easily calculable way. A continuous vacuum system covered the entire beam line.

The solid angle accepted by the system was 8.2 μsr and the momentum resolution was 0.90%.

B. Counter Array

Figure 1(b) shows the counter array, which was designed to detect and separate electrons, pions, kaons, protons, and muons. Here S_1–S_5 were plastic scintillators, C_1 and C_2 were Čerenkov counters, and D_1 and D_2 were microwave-gated photomultipliers, referred to in the literature as DCFEM's.[9] There is no further reference in this article to the DCFEM.

The spatial acceptance of the counter array was determined by S_2 and S_3 near the beam focus and S_1 which defined an angular aperture of ≈7 mrad.

C. Electron and Muon Separation

Scintillator S_4 detected showers produced by electrons interacting in the preceding lead. The thickness of lead was experimentally adjusted to be near the shower maximum for each momentum studied, and the discriminator on S_4 was set to reject single particles and accept only electron showers. Figure 2 illustrates the development of an electron shower by showing the counts obtained in S_4 (in coincidence with $S_1S_2S_3$) for various discriminator settings and various thicknesses of lead. The voltage of S_4 was set so that, with no lead, $S_1S_2S_3S_4$ did not count. The data were obtained with the 6-GeV/c secondary beam from the Be target, because at 6 GeV/c the Čerenkov counters (see Sec. II D) provided independent information about the fraction of electrons in the beam. The Čerenkov result was (44±2)% for the percentage of electrons in the beam, and we see that the curve with $\frac{7}{8}$ in. of lead forms a plateau at 46%, consistent with the Čerenkov results.

[9] O. L. Gaddy and D. F. Holshouser, Proc. IEEE 51, 153 (1963).

The plateau obtained at 6 GeV/c is not very impressive except in the context of the whole family of curves, because of a relatively small multiplicity at the shower maximum. As the momentum is increased, the number of particles at the shower maximum increases, and the plateau improves. This is illustrated in Fig. 3. Hence we believe the S_4-Pb system counts electrons with an efficiency of 98% or better. By studying the particle beams with plus charges where there is small positron percentage, we have determined that pions can trigger the S_4-Pb system approximately 4% of the time, probably by π^0 production with subsequent showers from the γ rays. Thus if we measure an electron percentage of 50%, it means that actually 48% of the beam was electrons. We have, therefore, a system which can separate electrons (or positrons) from all other particles at momenta for which our Čerenkov counters are not effective for this purpose (i.e., above 6 GeV/c).

Scintillator S_5, together with iron absorbers placed in front of it, measured the μ percentage in the beam. The diameter of S_5 was calculated to catch more than 95% of the muons, at 12 GeV/c, and to catch other particles <1% of the time, when 5 ft of iron was put in place. Figure 4 shows a measurement of $S_1S_2S_3C_1C_2S_5$ counts at 12 GeV/c as a function of the length of iron absorber. We see that muons form <1% of the beam.

D. Čerenkov Counters

The Čerenkov counters are relatively simple in construction, and weigh less than 20 lb each; two of them in coincidence are capable of a resolution comparable with that of the large counters of Kycia and Jenkins.[10] The Čerenkov counters consist of a 1-m-long steel pipe with a 1-in.-i.d. cylindrical glass tube, aluminized on the inside, mounted in the pipe by means of aluminum spacers. The fittings on both ends of the counter provided 50-mil Al windows for the beam to pass through, and at one end a 45-deg mirror of glass aluminized on one side turned the Čerenkov light through 90 deg where it exited from the pipe through a quartz window. For the threshold counter, we simply put the phototube against the quartz window. For the differential counter, a quartz lens with 16-in. focal length was put against the quartz window and a 100-mil-wide, 1.5-in.-diam annulus was mounted in the focal plane of the lens, with the phototube just behind the annulus. The Čerenkov angle prescribed by the differential counter was thus 2.7 deg.

The essential characteristic of the experiment which made it possible to use such simple counters was the small spatial extent (<$\frac{3}{4}$ in. diam) of the beam at the counter array. The counter was further kept small by the aluminized glass tube which confined the Čerenkov light to a 1-in. aperture without destroying any of its

[10] T. F. Kycia and E. W. Jenkins, in *Proceedings of the Conference on Nuclear Electronics, Belgrade, 1961* (International Atomic Energy Agency, Vienna, 1962), Vol. I, p. 63.

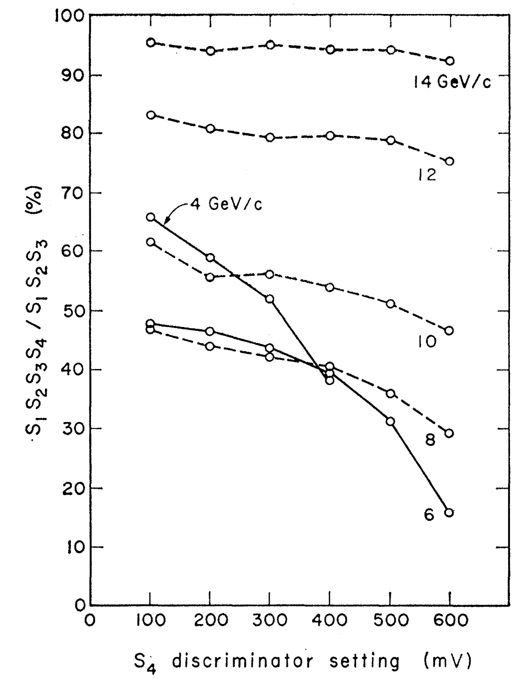

FIG. 3. Discriminator curves on the "shower counter" S_4. The plateau at low discriminator settings gets increasingly better as the momentum of the secondary beam increases. (Also, by the way, the electron fraction in the beam rises above 8 GeV/c.) The length of Pb in front of S_4 varied from $\frac{7}{8}$ in. at 4 GeV to $1\frac{1}{4}$ in. at 14 GeV.

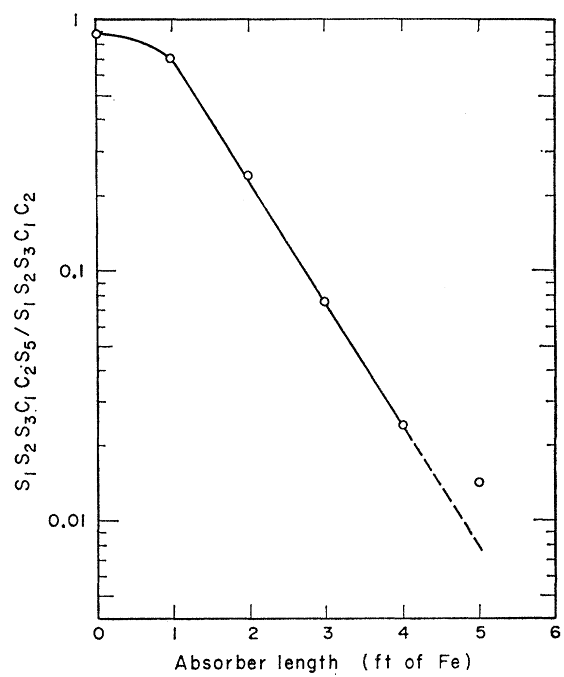

FIG. 4. A measurement of the μ fraction in the +12-GeV/c secondary beam for 18-GeV electrons on the Be target at 2 deg. The counter S_5 was used with various thicknesses of Fe in front of it. The attenuation of SIP follows the expected straight line until the very last point, which is 0.6% above the extrapolated line. We conclude that the μ fraction here is <1%.

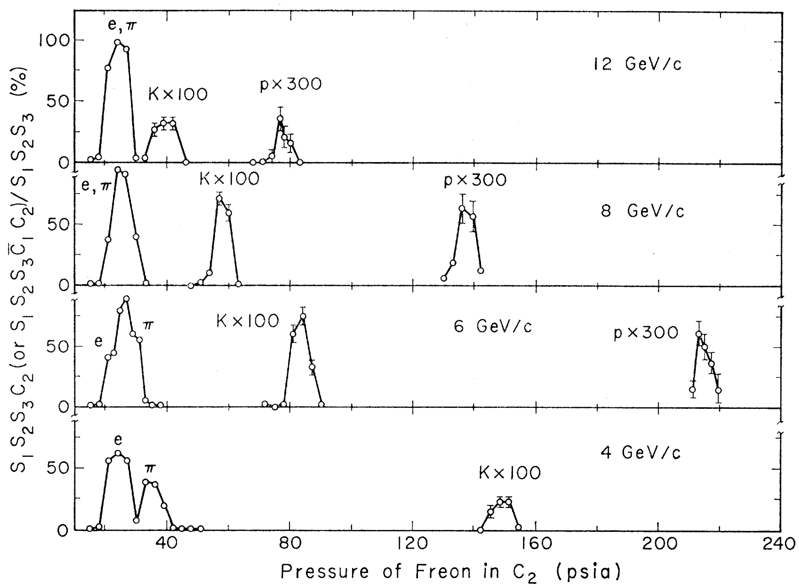

FIG. 5. The separation power of our Čerenkov counters. These data are for negatively charged particles. For data above the π peaks, C_1 was used to eliminate the tails of the e and π peaks as well as to eliminate accidentals. The width of the peaks, 8 lb/in.², corresponds to a $\Delta\beta=4\times10^{-4}$. From these raw recorded data, we can read directly the percentages of K, p, and, at the lower momenta, e and π in the beam.

useful characteristics. The small aperture also reduced the effects of chromatic aberration in the quartz lens.

Counter C_1 was filled with nitrogen gas at a pressure such that it would not count K's but only π-μ-e. Counter C_2 was filled with Freon 13 (a few times with N_2). To study the π-μ-e region, we recorded the coincidence counts $S_1S_2S_3$ and $S_1S_2S_3C_2$ at various pressures in C_2. Above the π-μ-e region, where we needed additional rejection against fast particles in order to clearly see the K and p peaks, we recorded $S_1S_2S_3\bar{C}_1C_2$ as a function of pressure in C_2. The separating power of these two counters is illustrated in Fig. 5. From these figures, which are raw recorded data, we can read off directly the percentages of K, p, and, at the lower momenta, π and e in the beam.

The resolution of the differential counter, as measured by $\Delta\beta/\beta$, can be determined from the width of the peaks as a function of pressure. A width of 8 lb/in.² corresponds to a $\Delta\beta/\beta=4\times10^{-4}$. The noticeable flat top on the peaks indicates that we could have improved the resolution somewhat by narrowing the annulus. However, the $\Delta\beta/\beta=4\times10^{-4}$ was adequate.

III. SCATTERING AND INTERACTION CORRECTIONS

The raw data were taken in the following way: First we measured the ratio of the number of coincidence counts in $S_1S_2S_3$ to the total charge integrated by the beam-monitor system in a given time interval. We call this ratio R_{mon}; it represents the total yield (of all particles we measure) per primary-beam electron. The percentage of a given particle in the beam is then obtained from graphs like those in Fig. 5. However, these raw numbers must be corrected for losses due to scattering and interaction in the material in the counter array. These losses, of course, mean that the R_{mon} should be increased by some amount, but they also mean that the percentage of a certain particle measured at a certain pressure in C_2 must be corrected, because $e^{\pm}$ have no strong interactions, and thus are affected differently by the material from π, K, and p.

Let us call R_{norm} the corrected ratio of $S_1S_2S_3$ to monitor integral. We use a very simple correction equation

$$R_{\mathrm{mon}}=R_{\mathrm{norm}}e^{-l/l_i}e^{-(\theta/\sigma)^2}, \tag{1}$$

where l is the length of material, l_i is the interaction length of the material, θ is the rms angle of scattering for the material, and σ is an angle characteristic of the geometry of the counter array, which we determine empirically.

The material in the counter array which affects R_{mon} includes S_1, S_2, windows and mirrors in C_1 and C_2, the vacuum pipe window, 2 m of air space, 50 psia N_2 in C_1, and a variable amount of gas in C_2. To find the effective l/l_i we must know l_i, the interaction length in g/cm², for all the materials. To find the effective θ^2 we must know the radiation length in g/cm² for all the materials. Numerically, Eq. (1) becomes

$$R_{\mathrm{norm}}=R_{\mathrm{mon}}\exp[(0.063+4.2\times10^{-4}P_G) + (21/p\sigma)^2(0.146+1.11\times10^{-3}P_G)], \tag{2}$$

where P_G is the pressure in psia of Freon in C_2, p is the momentum (in GeV/c) of the secondary beam, and σ is in mrad.

It is important the realize that Eqs. (1) and (2) are valid only for π, K, and p. For electrons, the interaction correction must be removed. This introduces a modification to the formula, giving

$$R_{\mathrm{norm}}=R_{\mathrm{mon}}e^{(\theta/\sigma)^2}[f^e+(1-f^e)e^{l/l_i}], \tag{3}$$

where f^e is the percentage of electrons in the beam. In the application of this formula we have used the ob-

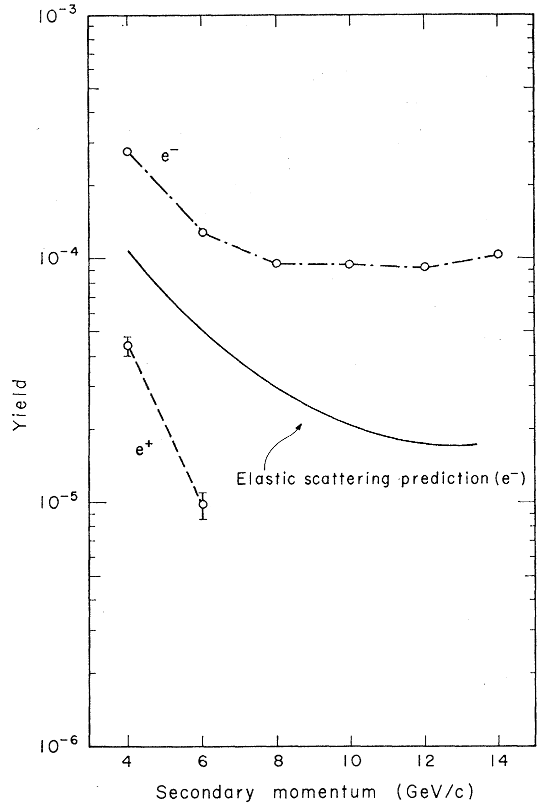

FIG. 6. Yields of $e^{\pm}$ for a 2-deg production angle and 18-GeV primary energy. Units are particles sr^{-1} $(GeV/c)^{-1}$ per incident electron on a 0.3-r.l. Be target. Errors shown are the algebraic sums of the statistical errors and nonstatistical fluctuations as described in the text. The over-all normalization of the data is believed to be accurate to $\pm 15\%$. The dashed lines are to eliminate confusion. The solid curve is the result of a theoretical calculation taking into account elastic scattering of the primary electrons (off Be nuclei and individual nucleons within the Be nuclei), and the energy loss of the electrons as they traverse the target (see Sec. V E). The much larger experimental yield ($\approx$factor of 5) arises from inelastic scattering (e.g., single-pion production).

served percentage of electrons rather than the corrected one; this is a very good approximation and makes calculation easier.

The equation for calculating the corrected percentage of electrons is

$$f_{\rm corr}{}^e = f_{\rm obs}{}^e [f_{\rm obs}{}^e + (1 - f_{\rm obs}{}^e) e^{l/l_i}]^{-1}, \tag{4}$$

where l/l_i is evaluated for the pressure in C_2 at which the measurement of $f_{\rm obs}{}^e$ was made. The equation for calculating the corrected percentage of π, K, or p is

$$f_{\rm corr} = f_{\rm obs} e^{l/l_i} [f_{\rm obs}{}^e + (1 - f_{\rm obs}{}^e) e^{l/l_i}]^{-1}, \tag{5}$$

where l/l_i is evaluated at the pressure in C_2 corresponding to the peak for the particle in question. In these last two formulas we have again used $f_{\rm obs}{}^e$ where we should have used $f_{\rm corr}{}^e$; the difference in the correction factor is negligible.

In order to determine σ we need only compare $R_{\rm mon} \times f_{\rm obs}{}^e$ at two different pressures in C_2. Since $R_{\rm norm} \times f_{\rm corr}{}^e$ stays the same by definition, we may solve for σ. Using data from a 2-deg production angle, 18-GeV incident electrons, and the Be target, we find for *both* the 4- and 12-GeV/c secondary beams that $\sigma = 5.2$ mrad. The fact that the same value of σ is valid for the extremes of momenta, and that the value of σ is quite reasonable for the counter geometry, gives us confidence that the equation has physical meaning.

Once σ is determined we can check the coefficient of P_G in the first parenthesis of the exponential of Eq. (2) by comparing $R_{\rm mon}$ at two different pressures in C_2. At both 4 and 12 GeV/c this coefficient checks well with experimental values. Thus again we are given confidence that the equation is useful. The total scattering-plus-interaction correction is typically 15%.

IV. EXPERIMENTAL YIELDS

All results are shown in Table I. The measurements have been corrected for scattering and interaction losses in the material of our counter array, and for the decay of pions and kaons, in their flight from target to detector. The scattering and interaction corrections were typically 15%. To the statistical error associated with each measurement, we have added algebraically an error of $\approx 2\%$, which reflects nonstatistical fluctuations

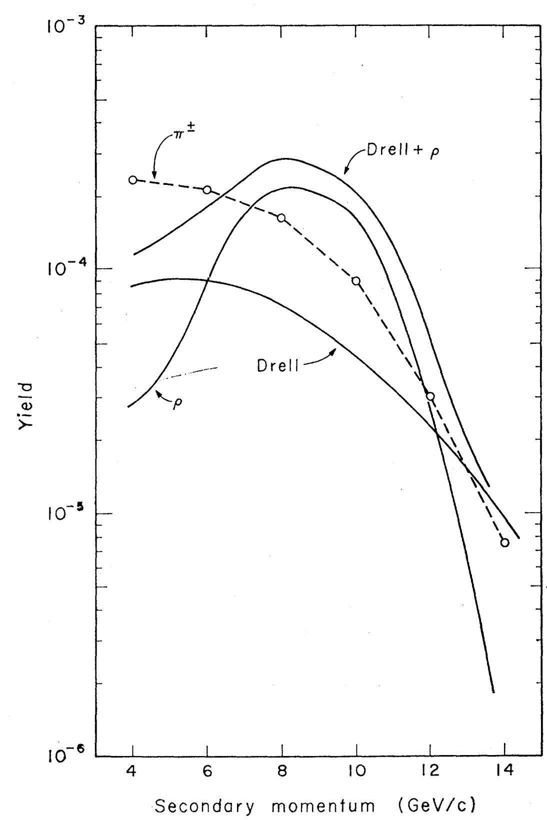

FIG. 7. Yields of $\pi^{\pm}$. The units, production angle, primary energy, target, and error determination are identical to those in Fig. 6. The solid curves are π yields from ρ production and from the Drell process, as calculated in Ref. 15.

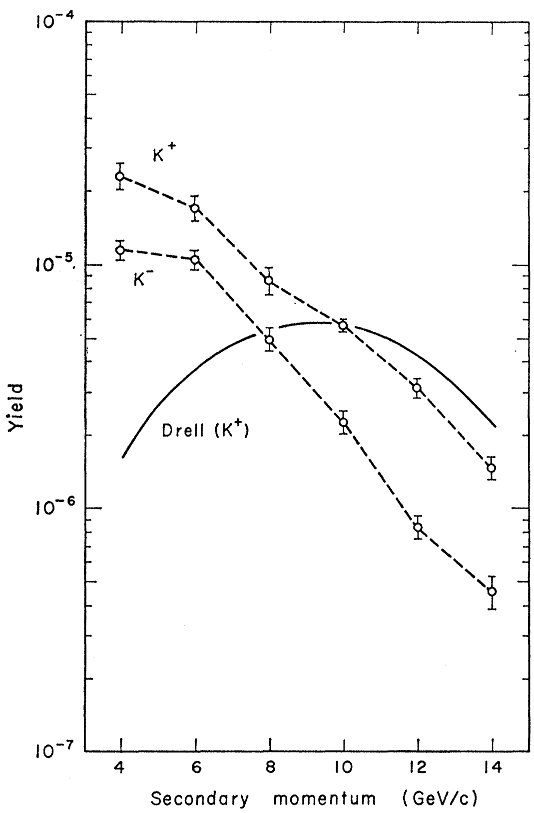

FIG. 8. Yields of $K^{\pm}$. The units, production angle, primary energy, target, and error determination are identical to those in Fig. 6. The solid curve is the K^+ yield from the Drell process as calculated in Ref. 15; the theoretical K^- yields are everywhere 30% lower than the theoretical K^+ yields calculated according to the Drell process.

of unknown origin in the ratio of $S_1S_2S_3$-to-monitor charge integral.

If the ratio of any two numbers in Table I that are associated with the *same target* is taken, then the error in that ratio is correctly obtained from the errors in the table. If the ratio of two numbers associated with different targets is taken, then an additional error of 3% must be added to the error from Table I due to uncertainty in the ratio of beam-monitor efficiency for the different targets (see Sec. II A).

We believe that the over-all normalization of the data is accurate to $\pm 15\%$ (5% from beam-monitor current normalization and 10% from solid-angle and momentum-bite uncertainty). That is, a lone number taken from Table I must have an additional 15% error added to compare with any absolute prediction.

Figures 6–9 show the 2-deg yields from Be at 18-GeV primary energy as a function of secondary momentum for $e^{\pm}$, $\pi^{\pm}$, $K^{\pm}$, and $p^{\pm}$. Figures 10–12 show representative angular distributions of yields from 18-GeV primary electrons. In Fig. 10, the two points at 0.5 and 1 deg were taken from Boyarski *et al.*[11] It was necessary to correct their data from 16- to 18-GeV primary energy as well as to correct for a different target length (0.6 r.l.). The details of this conversion calculation are given in Sec. V G. Comparison with the 0-deg data of Barna *et al.*[12] is not shown, since rather large and uncertain normalization factors would be needed to convert their 1.8-r.l. data to a 0.3 r.l.

The relationship between results from the Be target and results from the Fe target gives some indication about the dependence of the yields on the characteristics of the nucleus in the target. If we assume that the cross section (σ) for production of secondaries is proportional to A^n, where A is the at. wt of the nucleus, then an expression for n in terms of the yields is

$$n = 1 + \ln(r_{\mathrm{Be}} Y_{\mathrm{Fe}} / r_{\mathrm{Fe}} Y_{\mathrm{Be}}) / \ln(A_{\mathrm{Fe}} / A_{\mathrm{Be}}),$$

where r_{Be} (r_{Fe}) is the radiation length of Be (Fe) in g/cm^2, and A_{Be} (A_{Fe}) is the at. wt of Be (Fe). Thus a given ratio of yields corresponds uniquely to a value for n. Of course, there is no guarantee that the cross section is proportional to any one power of A. In fact, it might depend on Z rather than on A, as elastic electron scattering does. However, this technique at least allows us to discuss the dependence of the yields

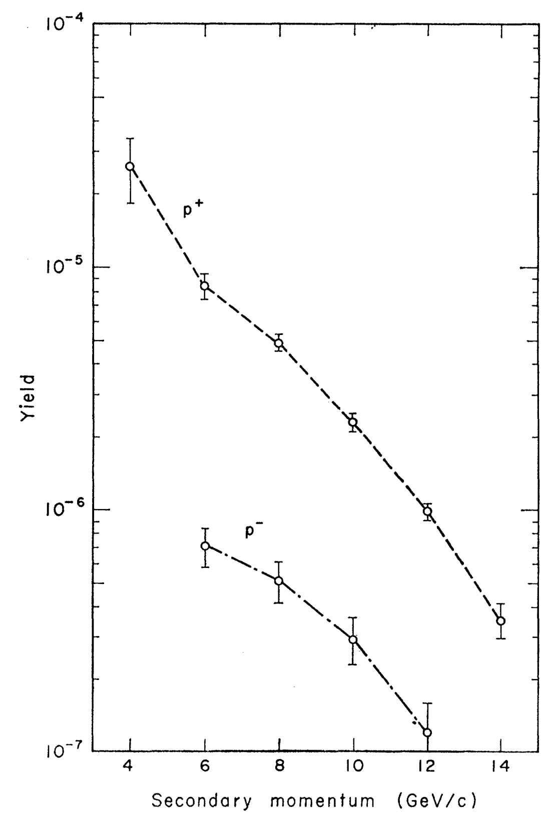

FIG. 9. Yields of $p^{\pm}$. The units, production angle, primary energy, target, and error determination are identical to those in Fig. 6.

[11] A. Boyarski, F. Bulos, W. Busza, D. Coward, R. Diebold, J. Litt, A. Minten, B. Richter, and R. Taylor, Phys. Rev. Letters 18, 363 (1967).

[12] A. Barna, J. Cox, F. Martin, M. L. Perl, T. H. Tan, W. T. Toner, and T. F. Zipf, Phys. Rev. Letters 18, 360 (1967).

on the target nucleus in Sec. V F. Figure 13 shows the results for the ratio of yields from Be and Fe, along with the scale of n corresponding to each ratio.

The ratios of yields from the Be-Fe-combination target and the Be target are shown in Fig. 14. We note that adding a 1-cm length of iron to a 10-cm Be target increases the yields by a factor of 2 or 3. The significance of these results is discussed in Sec. V B.

V. THEORETICAL INTERPRETATION OF YIELD RESULTS

A. Introduction

It is generally believed that production of strongly interacting particles (SIP) by an electron beam is a two-step process, with the electrons forming real photons by the bremsstrahlung process, followed by the interaction of the photons with the target nuclei. The analogous process with a virtual photon, usually called electroproduction, is important only for targets very much shorter than ours. Consideration of the two-step process allows us to predict roughly the dependence of yields on primary electron energy and on target length, and also derive some rough cross sections, as discussed in Sec. V B.

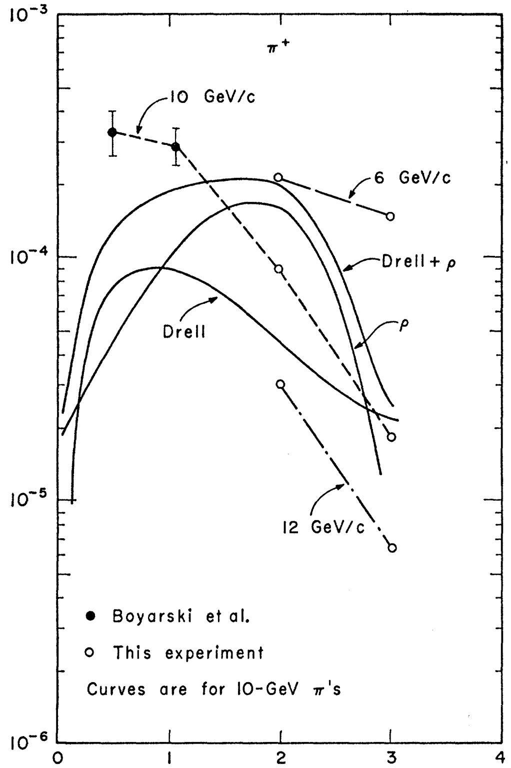

FIG. 10. Representative angular distributions for π^+ from 18-GeV primary electrons. The units, primary energy, target, and error determination are identical to those in Fig. 6. The 10-GeV/c distribution contains the *adjusted* data of Boyarski *et al.* (Ref. 11); see Sec. V G. The solid curves are π yields from the Drell process and from ρ production, as calculated in Ref. 15.

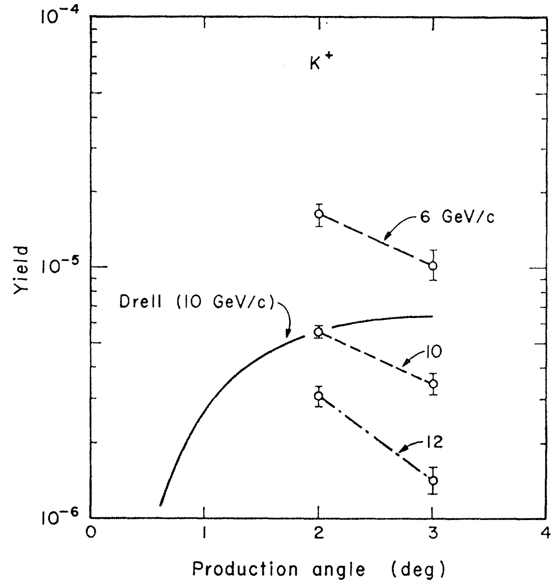

FIG. 11. Representative angular distributions of K^+. The units, primary energy, target, and error determination are identical to those in Fig. 6. The solid curve is the 10-GeV/c yield from the Drell process, as calculated in Ref. 15.

Since real photons are incident on the nuclei, we need a theory of the photon-nucleus interaction to interpret the SIP yields; the mechanisms considered in this section are the Drell mechanism, ρ-meson production (for pions), and photodisintegration (for protons). The results, discussed in Secs. V C and V D, indicate that the pion, kaon, and antiproton yields are explained, roughly, by the Drell and ρ processes, and the proton yields could be explained by the combination of Drell and photodisintegration processes.

We have obtained some yields for particles that are not strongly interacting, namely, electrons. In Sec. V E, we have attempted to calculate the electron yields from elastic scattering of the incoming electrons, either with the nucleus as a whole, or with individual nucleons inside the nucleus. We find that the calculated yields are only about $\frac{1}{5}$ the observed yields, indicating that inelastic processes, such as pion production, are dominating the electron scattering in this region of energy and angle.

Finally, we compare our results from the iron and beryllium targets in terms of the dependence of the yields on A, the at. wt of the nucleus, in Sec. V F.

B. Implications of the Bremsstrahlung Spectrum

As the primary electron beam proceeds through the Be target, it creates real photons of a known energy spectrum and intensity. Calculations of the number of photons in a given energy interval, and at a given depth in the target, have been done by Tsai and Whitis.[13] If we knew the cross section for a photon producing a particular secondary particle as a function of photon

[13] Y. S. Tsai and V. Whitis, Phys. Rev. 149, 1250 (1966).

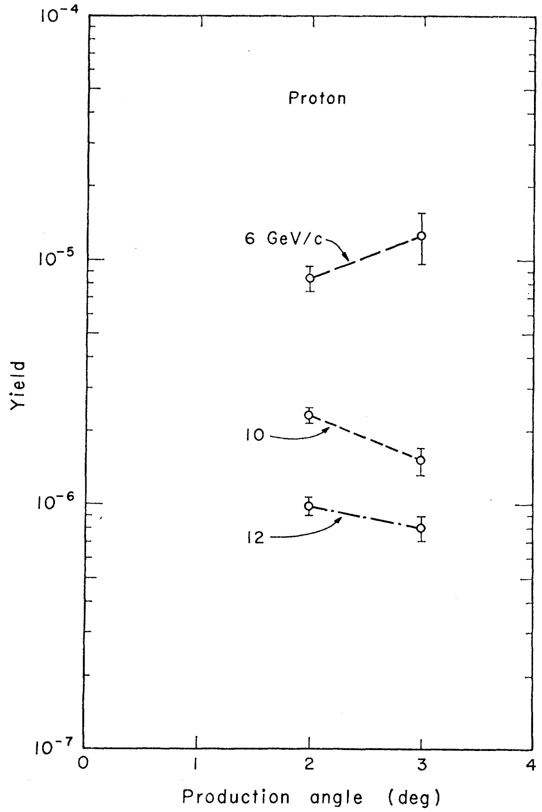

FIG. 12. Representative angular distributions of protons. The units, primary energy, target, and error determination are identical to those of Fig. 6.

energy, then we could combine our knowledge of the photon spectrum with this cross section to produce a yield. This is what Tsai and Whitis have done with the Drell mechanism and ρ-production cross sections treated in the next section.

However, suppose we know nothing about the cross section except the obvious fact that a photon with momentum p cannot produce a secondary particle with energy greater than p. Figure 15 illustrates the bremsstrahlung spectra integrated over the length of Be in the target, for three cases.

First, let us compare curves (b) and (c). The path length of photons is much greater in the long target than in the shorter one, but the shapes of the energy spectra are quite similar. Therefore, we expect the relative yields to be rather independent of specific production mechanisms; the yield of 10-GeV secondaries produced in the long and short targets should be roughly in proportion to the integral of curves (b) and (c) in Fig. 15 above 10 GeV/c. Table II and Fig. 14 show a comparison between predictions for the ratios of Be and Be-Fe yields and the experimental results for the SIP. We see that rough agreement is obtained.

Second, we compare curves (a) and (c). Here the photon-pathlength distribution for 18-GeV electrons differs from that for 16-GeV electrons only in the

TABLE II. Ratios of yields from the Be-Fe target (0.6-r.l. Fe followed by 0.3-r.l. Be) to yields from the 0.3-r.l. Be target, with predictions calculated from the expected photon distributions in the target, as explained in Sec. V B. The primary electron energy was 18 GeV, and the production angle was 2 deg.

Charge and secondary momentum (GeV/c)	Prediction	(Be-Fe yield/Be yield) Experiment Pion	Kaon	Proton
+6	2.84	2.5±0.1	2.3±0.4	2.0±0.3
+8	2.64	3.0±0.1	2.9±0.5	3.0±0.4
+12	2.24	2.2±0.1	2.3±0.3	2.5±0.3
−6	2.84	2.7±0.2	2.3±0.4	2.3±0.5
−12	2.24	2.1±0.3	2.4±0.4	1.6±0.8

16–18-GeV region. Thus if the cross section for producing a certain secondary varies rapidly with photon energy, we would not expect the method of integrating the path length over energy to give an accurate prediction. However, the comparison between predictions for the ratios of 18- and 16-GeV yields and the experimental results, shown in Table III, again indicates rough agreement. This seems to indicate that the cross sections are relatively constant as a function of photon energy.

We have used this theory to convert the data given in Ref. 11 for 10-GeV/c π^+ yields, in order to plot their

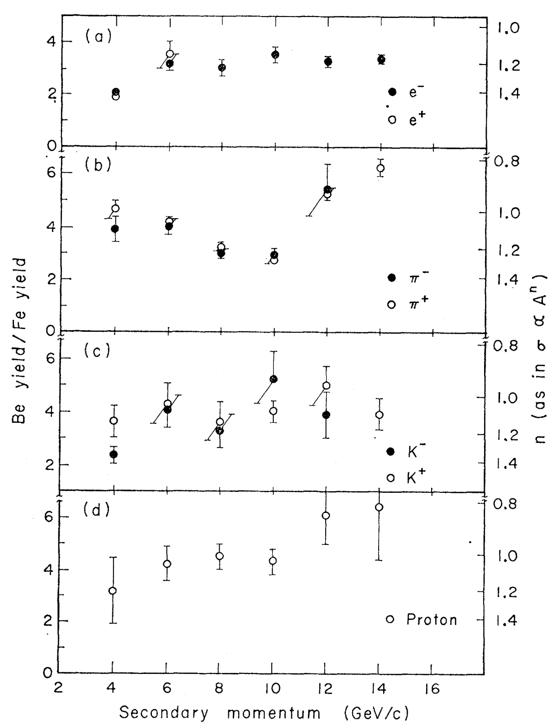

FIG. 13. A dependences of the yields. The ratio of the Be-target yield to the Fe-target yield is plotted as a function of momentum for $e^{\pm}$, $\pi^{\pm}$, $K^{\pm}$, and p. On the assumption that the cross section for a photon on a nucleus, to produce a given particle, is proportional to A^n, where A is the atomic weight of the nucleus, there is a unique correspondence between a ratio and a value of n. The scale of n is shown on the right.

TABLE III. Ratios of yields from 18-GeV electrons to yields from 16-GeV electrons, with predictions calculated from the expected photon distributions in the target, as explained in Sec. V B. The target was 0.3 r.l. of Be, and the production angle was 3 deg.

Charge and secondary momentum (GeV/c)	Prediction	18-GeV yield/16-GeV yield Experiment Pion	Kaon	Proton
+10	1.29	1.25±0.1	1.35±0.2	1.4 ±0.3
+12	1.49	1.8 ±0.1	1.35±0.2	2.5 ±0.4
−12	1.49	1.4 ±0.2	1.55±0.3	1.55±1.0

results in Fig. 10. We have converted from their 16-GeV electron beam to our 18-GeV electron beam (a factor of 1.3), and from their 0.6-r.l. target to our 0.3-r.l. target (a factor of 0.30), so that we multiplied their data at both 0.5 and 1 deg by 0.38. From our conclusions above we estimate the error in this conversion factor to be less than 30%.

By subtracting the yields of 16-GeV electrons from the yields of 18-GeV electrons, we can form a crude idea of the actual cross sections for secondary-particle production by monochromatic 17-GeV photons. The integrated path length for the *difference* is $\approx 3.6\times10^{-3}$ r.l./electron, which means that a difference between 18- and 16-GeV yields of one-particle GeV^{-1} sr^{-1} (10^7 incident electrons)$^{-1}$ from the Be target represents a cross section of 7 μb sr^{-1} (GeV/c)$^{-1}$. For example, the cross section for 3-deg production of 12-GeV/c π^- by 17-GeV photons on Be is 0.1 mb sr^{-1} (GeV/c)$^{-1}$. For comparison we note that the cross section for 0-deg (5-deg) production of 12-GeV/c π^- by 18.8-GeV protons[14] on Be is 17 (0.2) mb sr^{-1} (GeV/c)$^{-1}$.

C. Predictions of Drell $+\rho$ for π, K, p, and $\bar{p}$ Yields

Calculations of the yields of pions and kaons from the Drell process, and also of the pion yields from ρ-meson production, have been performed by Tsai and Whitis.[15] Their results at 2 deg and as a function of secondary momenta, shown in Figs. 7 and 8, give order-of-magnitude agreement with the experimentally observed yields. Their prediction of the angular distributions at fixed secondary momenta, shown in Figs. 10 and 11, are similar to the observed angular distributions, except that the experimental distributions seem to decrease with increasing angle less rapidly than the theoretical ones.

Both the Drell and ρ processes predict that the ratio of the yields of π^+ and π^- is unity for all secondary momenta. This is observed experimentally. However, the Drell process predicts that K^+/K^- is 1.3, but the observed ratio varies between 1.6 and 3.7. This appears to imply that the process $\gamma p\rightarrow K^+\Lambda$ (Σ) is important; however, this process has been calculated[6] to be 2–3

[14] D. Dekkers, J. A. Geibel, R. Mermod, G. Weber, T. R. Willitts, K. Winter, B. Jordan, M. Vivargent, N. M. King, and E. J. N. Wilson, Phys. Rev. **137**, B962 (1965).

[15] Y. S. Tsai and V. Whitis (private communication).

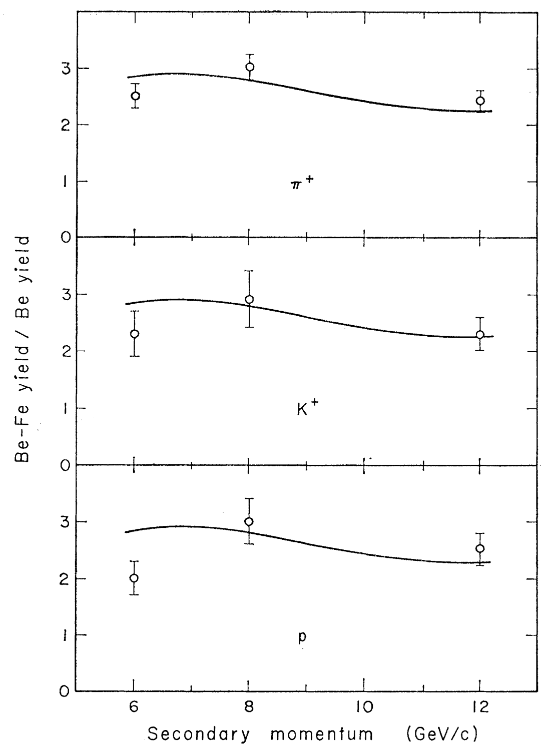

FIG. 14. Ratio of the Be-Fe-target yield to the Be-target yield, as a function of momentum, for π^+, K^+, and p. We note that adding a 1-cm thickness of iron to the front of a 10-cm thickness of Be increases the yield by a factor of 2 or 3. The continuous curves are predictions based on the known photon spectra in the targets (see Sec. V B).

orders of magnitude lower than necessary to explain the observed excess of K^+ over K^-. Another process[6] which could produce more K^+ than K^- is $\pi p\rightarrow K^+\Lambda$ (Σ) taking place inside the same nucleus in which the π is produced by a γ. Although data on the A dependence of the yields should shed light on this possibility, the results in Sec. V F are not accurate enough to confirm or disprove that K^+'s are being produced by pions.

The quantitative disagreement between Drell $+\rho$ and experiment in the dependences of π and K yields on secondary momentum and production angle may be understood qualitatively by invoking one other mechanism: final-state interactions. If, after the Drell process has operated to produce a π or K, the π or K interacts with the rest of the nucleus, two effects will occur: (a) The angular distribution of the secondary particle will be broadened by scattering, and (b) the distribution of momenta of the secondary particle will favor lower momenta than the simple Drell process would indicate, because of energy loss in the scattering. These two effects, qualitatively, are indeed seen.

The $\bar{p}$ yields, shown in Fig. 9, are consistent with the order-of-magnitude prediction of the Drell mechanism.[6] However, the Drell process predicts that $p/\bar{p}$ is 1, whereas experimentally we have $p/\bar{p}\approx 10$. Hence some

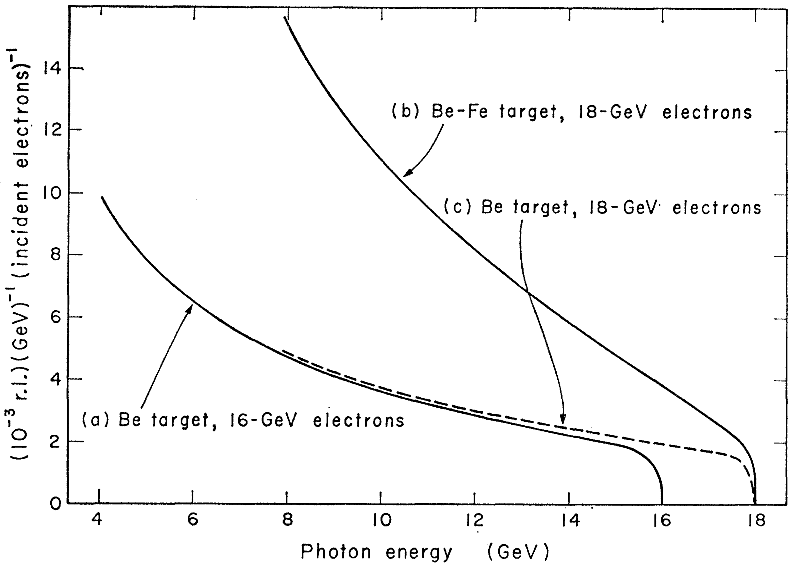

FIG. 15. The photon-path-length spectra for electrons traversing different targets: (a) 16-GeV electrons through 0.3 r.l. of Be; (b) 18-GeV electrons traversing 0.6 r.l. of Fe followed by 0.3 r.l. of Be; (c) 18-GeV electrons traversing 0.3 r.l. of Be. "Path length" is a simple device for expressing the probability of a photon's being in proximity to a nucleus. To calculate a yield, one must fold in the (in general, energy-dependent) cross section for producing the particle of interest. A path length of 1 r.l. of Be is equivalent to 4.1 events/b.

other mechanism is operating in the proton case. A possibility, photodisintegration, is discussed in Sec. V D.

Hence the $\pi^{\pm}$, K^{-}, and $\bar{p}$ yields are qualitatively explained by the combination of the Drell process and ρ production, with the addition of final-state interactions. We are forced to say "qualitatively" presumably only because we cannot calculate the final-state interactions. The K^{+} and p yields appear to have different mechanisms operating, in the K^{+} case perhaps associated production by pions, and in the proton case perhaps photodisintegration.

D. Proton Yields–Photodisintegration

The Drell mechanism, in fact just about any mechanism by which a proton-antiproton pair is created, predicts equal yields for protons and antiprotons. The antiproton yields are a reasonable order-of-magnitude for the Drell process,[6] but the proton yields, shown in Fig. 9, are one order-of-magnitude higher.

Drell[7] has suggested that photodisintegration can account for the proton yields. In this mechanism, the photon finds a proton with a very large momentum inside the nucleus, and can thus produce a proton with large momentum transfer without depressing the amplitude with a small form factor. This model therefore depends crucially on the probability of the photon's finding a proton with high momentum in the nucleus; in other words, it depends crucially on what is assumed for the wave function of the nucleus.

Extremely rough calculations[16] indicate the following: If an exponential wave function is assumed, there are enough high-momentum components to predict a proton yield of the right order of magnitude. However, if a shell-model wave function is assumed, then the amount of high-momentum components is entirely too small to account for the observed yields.

Until more is known about the nuclear wave functions we can only guess that photodisintegration, or similar processes which might produce some extra pions but do not produce antiprotons, are active here.

E. Electron Yields

The mechanism for producing secondary electrons is quite different from that which produces SIP. First we realize that electrons of all energies are produced in the forward direction as the primary electrons lose energy by bremsstrahlung. However, neither the bremsstrahlung process nor multiple scattering in the target is capable of sending secondary electrons off at angles of 2 or 3 deg. Only a single strong collision of the secondary electron with one nucleus is capable of yielding significant amounts of secondary electrons at large angles.

It is tempting to predict that among the single-scattering events, only elastic scattering, either off the nucleus as a whole (coherent), or off a single nucleon within the nucleus (incoherent), is important. If that were the case then we could describe the production of secondary electrons in the following way: A primary electron enters the target and gradually loses energy by bremsstrahlung radiation until it emerges at the end of the target with the secondary momentum we are studying. (The probability that the electron will emerge with any given momentum has been calculated.) Somewhere along its path through the target the electron suffered an elastic collision (no energy loss) that provided a sufficient impulse for it to emerge from the end of the target at a production angle of 2 (or 3) deg.

To calculate the yields from this whole process, we first need the elastic electron-nucleus scattering cross section which is

$$d\sigma/d\Omega = F^2(d\sigma/d\Omega)_R,$$

[16] J. Gillespie (private communication).

where $(d\sigma/d\Omega)_R$ is the Rosenbluth cross section, and

$$F^2=ZF_p^2+Z(Z-1)F_{Be}^2,$$
$$F_p=1/(1+1.4Q^2)^2,$$
$$F_{Be}=1/(1+26Q^2),$$

where Q^2 is the 4-momentum transfer in (GeV)^2 (form factors are from Ref. 17).

We now make the reasonable approximation, for electrons emerging from a target of length t_0 with energy E_f, that their energy as a function of depth in the target is

$$E(t)=E_0(E_f/E_0)^\alpha,$$

where $\alpha=t/t_0$, and E_0 is the primary electron energy (this equation is exact on the average but of course is not true for each individual electron). Then the effective cross section for a single scattering is

$$\left(\frac{d\sigma}{d\Omega}\right)_{\text{eff}}=\int_0^1\frac{d\sigma(E)}{d\Omega}d\alpha.$$

This integration has been carried out for the Be target and a production angle of 2 deg, and the result is presented as the curve in Fig. 6. We see that the theory is a factor of ≈ 5 too low. We must conclude that other single-scattering processes are dominating the electron yields (e.g., single-pion production).

F. General Interpretation of A Dependences

Since we obtained data from targets of Be and Fe with the same radiation length in each, we have a measure of the dependence of the yields on A, as explained in Sec. IV B. It is rather presumptuous of us to take two points from a perhaps complicated curve, and connect them with a straight line, but lacking more information we hope we can deduce something of value from this approximation.

The pion results are shown in Fig. 13(b). We note that the π^+ and π^- results are identical within errors, a reflection of the fact that the yields of π^+ and π^- are equal for both the Fe and Be targets. We also note that n is tending to a value less than 0.8 at high energy. We can understand this in the following way: Any pion which is formed inside a nucleus must progress through nuclear matter, where it has a good chance of interacting on its way out. For pions produced with the maximum possible energy, only those that are produced on the back surface of the nucleus will be able to escape with no loss of energy. Hence the high-energy limit of n in Fig. 13(b) should be 0.67. The Drell mechanism predicts 0.67 also, but for all energies, because the "almost real" pion interaction with the nucleus should have the same A dependence as a real pion interaction. However, models have shown that the virtuality of the exchanged pion can change the A dependence.[18]

The K and p results are shown in Figs. 13(c) and 13(d). We evidently must restrict ourselves to saying that roughly $\frac{2}{3}<n<\frac{4}{3}$. We would wish to have better results in the K case, since we might then reach a conclusion as to whether K^+'s are produced by $\pi p\rightarrow K^+\Lambda$ (Σ) inside nuclei where pions are formed, but our data are insufficient.

The electron results are shown in Fig. 13(a). Here we do not expect the cross section to depend on A but rather on Z. However, since $A_{Be}/A_{Fe}=Z_{Be}/Z_{Fe}$, we can regard n as a power of Z. We see that n is between 1 and 2 but closer to 1, which we interpret to indicate that coherent nuclear interactions are taking place but incoherent processes are dominant.

The shape of the A-dependence curve as a function of energy, which is well determined for e and π, remains to be explained quantitatively.

ACKNOWLEDGMENTS

We thank Roger A. Gearhart and Todd Hauser of the Lawrence Radiation Laboratory for their great efforts in the preparation and running of the experiment. We wish to express appreciation to the University of Hawaii Physics Department for its interest and help during the experiment. We are grateful to many people at the Stanford Linear Accelerator Center, but especially to Dr. Y. S. Tsai and V. Whitis for their extensive theoretical calculations, and to Professor S. D. Drell for several stimulating discussions. We wish to thank the Research Area Department for skillful operation of the accelerator and associated equipment. The assistance and cordiality of the entire SLAC staff is gratefully acknowledged. Finally, it is a pleasure to thank Professor Luis Alvarez for his encouragement and support.

[17] R. Hofstadter, Ann. Rev. Nucl. Sci. **7**, 231 (1957).

[18] J. S. Bell, Phys. Rev. Letters **13**, 57 (1964).